Title: A facile approach to build $Bi_2O_2CO_3$/PCN nanohybrid photocatalysts for gaseous acetaldehyde efficient removal

Authors: Qitao Zhang, Saisai Yuan, Bin Xu, Yangsen Xu, Kuanhong Cao, Zhengyuan Jin, Chuntian Qiu, Ming Zhang, Chenliang Su, Teruhisa Ohno

PII: S0920-5861(18)30359-6
DOI: https://doi.org/10.1016/j.cattod.2018.03.071
Reference: CATTOD 11354

To appear in: *Catalysis Today*

Received date: 30-11-2017
Revised date: 13-3-2018
Accepted date: 28-3-2018

Please cite this article as: Zhang Q, Yuan S, Xu B, Xu Y, Cao K, Jin Z, Qiu C, Zhang M, Su C, Ohno T, A facile approach to build $Bi_2O_2CO_3$/PCN nanohybrid photocatalysts for gaseous acetaldehyde efficient removal, *Catalysis Today* (2010), https://doi.org/10.1016/j.cattod.2018.03.071

A facile approach to build $Bi_2O_2CO_3$/PCN nanohybrid photocatalysts for gaseous acetaldehyde efficient removal

Qitao Zhang [a,§], Saisai Yuan [b,c,§], Bin Xu[c,d], Yangsen Xu[a], Kuanhong Cao[c], Zhengyuan Jin[a], Chuntian Qiu[a,*], Ming Zhang [c,d], Chenliang Su[a] , Teruhisa Ohno[b,e,*]

[a] SZU-NUS Collaborative Center and International Collaborative Laboratory of 2D Materials for Optoelectronic Science & Technology, International Collaborative Laboratory of 2D Materials for Optoelectronics Science and Technology of Ministry of Education, College of Optoelectronic Engineering, Shenzhen University, Shenzhen 518060, China

[b] Department of Applied Chemistry, Faculty of Engineering, Kyushu Institute of Technology, Kitakyushu 804-8550, Japan

[c] School of Chemistry and Chemical Engineering, Yangzhou University, Yangzhou 225002, China

[d] Test Center, Yangzhou University, Yangzhou 225002, China

[e] JST, ACT-C, 4-1-8 Honcho Kawaguchi, Saitama 332-0012, Japan

[§]These authors contributed equally to this work

* Corresponding author at: qiuct@szu.edu.cn (C.Qiu), tohno@che.kyutech.ac.jp (T. Ohno).

Graphical Abstract

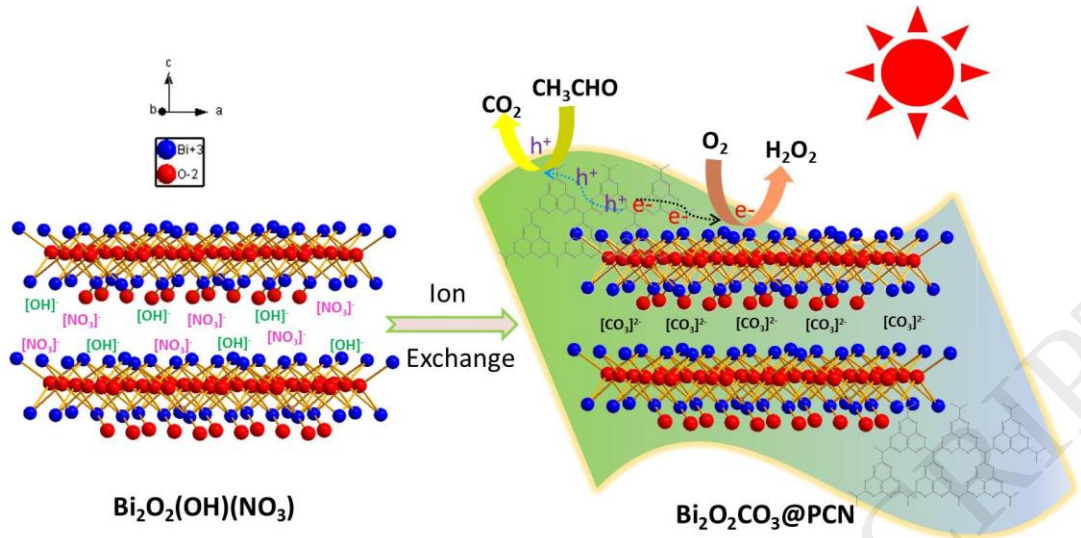

Highlights

● A cost-effective heterojunction photocatalyst was fabricated by solvothermal treatment.

●The photo-degradation CH_3CHO performance was enhanced greatly.

● 0.5 $Bi_2O_2CO_3$@PCN presented the best photoactivity among the as-prepared photocatalysts.

●$Bi_2O_2(OH)(NO_3)$ was fully converted to $Bi_2O_2CO_3$ by ion exchange reaction with PCN.

●BIOC@PCN formation and its photocatalytic mechanism were proposed.

Abstract

Constructing heterojunction between two semiconductors is a cost-effective pathway to fabricate efficient photocatalysts for environmental remediation and energy-related applications, which is with profound significance and high desirability to contemporary era. In this work, we demonstrate an extremely facile approach to couple bismuth subcarbonate with polymeric carbon

nitride (denoted as BIOC@PCN) by ion exchange between home-made rose-like $Bi_2O_2(OH)(NO_3)$ (denoted as BION) and PCN bulks at 433K solvothermal condition. PCN bulks play multi-roles in this ingenious one-pot method. Firstly, PCN bulks guarantee the negatively charged surface to anchor plentiful bismuth precursor salts. More importantly, solvothermal treatment affords a weak basic and sufficient CO_3^{2-} ions environment to promote the following ion exchange reaction. The evolution of morphology, components and structure from rose-like BION to BIOC@PCN were symmetrically characterized by means of SEM, HR-TEM, XRD, FTIR, TG, UV-vis, BET-BJH and XPS. The as-prepared nanohybrid photocatalyst (0.5BIOC@PCN) presents optimal photocatalytic performance for gaseous acetaldehyde removal, which is showing 10, 6.5 and 2 times higher than that of the PCN-Bulk, BION and mechanical mixed BIOC/PCN counterparts, respectively. Transient photocurrent response and EPR results further verify the validity of the established heterojunction of BIOC@PCN in facilitating the separation of charge carriers. The performance improvement gains from the efficient separation of charge carriers in BIOC@PCN heterojunction, manifested by PL spectra, transient photocurrent response and EPR results. In this study, a facile and cost-effective approach to build PCN-based nanohybrid photocatalysts for gaseous acetaldehyde efficient removal was established.

Keywords: $Bi_2O_2(OH)(NO_3)$, $Bi_2O_2CO_3$, polymeric carbon nitride, heterojunction, ion exchange, CH_3CHO photooxidation.

1. Introduction

Photocatalytic oxidation achieved by solar energy and semiconductors, as one of the most sustainable and efficient AOPs (advanced oxidation processes) to remediate air/water pollution, has drawn huge attention in contemporary society [1-5]. Undeniably, TiO_2 semiconductor photocatalyst has turned out to be the most representative since its pioneering research by Fujishima and Honda in 1972 [1]. With a relatively big bandgap (E_g values of rutile, anatase and brookite phases are larger than 3 eV), TiO_2 is a typical UV-light-driven photocatalyst. But, UV light accounts for only 4% in the whole solar illumination spectra, while visible light (400-800nm) is the dominate proportion (50%). Therefore, such fatal drawback greatly impedes its further

practical applications in novel energy production and environmental remediation. Up to now, numerous modification approaches have adopted to fabricate visible-light-driven (VLD) TiO_2 photocatalysts [7,8]. For instance, non-metals doping (C, N, O, S), metal ions deposition (Ti3+, Fe3+, Cu2+), dyes sensitization, and surface plasmon resonance (SPR). Regardless of the stability of above-mentioned VLD TiO_2, the optimal balance between costs and benefits is also somewhat difficult to satisfy. Shifting from the traditional inorganic metal oxide-based photocatalysts, the research of polymeric materials has attracted exponential amplification in recent years [9,10]. For instance, polymeric carbon nitride, as a new star since it was first launched in 2009 as a metal-free polymeric photocatalyst to split water into hydrogen [10], has emerged as a promising desirable candidate for industrially used catalysts. PCN possess high chemical stability, moderate bandgap value (ca. 2.7 eV), and suitable band position for artificial photosynthesis, such as selective photoreduction or photooxidation of organic molecules, water-splitting to H_2/O_2 and CO_2 conversion [11-13]. Most importantly, it can be prepared by a facile pyrolysis nitrogen-rich precursors' method with low cost and in high yield. One thing here to note is the misleadingly classed such polymeric carbon nitride as 'graphitic carbon nitride', 'graphitic CN' or 'g-C_3N_4' in most scientific literatures, strongly recommended referring to melon either by its non-systematic name or as poly (aminoimino) heptazine, or as PCN by Kessler et al[14]. Therefore, for the purpose of clarity, we denoted the as-prepared polymeric carbon nitride as PCN in the following part.

Nevertheless, the small specific surface area (ca.10 m^2/g) and fast recombination rate of photogenerated charge carriers of PCN greatly hinder its photocatalytic performance enhancement. Therefore, various physicochemical modification approaches have been used to overcome above-mentioned drawbacks. So far, metal/nonmetal heteroatom doping [15-19], metal-complex/dye-sensitization [20], heterojunction structure formation [21-27] and ultrasonic exfoliation have been adopted to boost the photocatalytic performance of PCN [28, 29]. Among the various approaches, constructing the heterojunction interaction was proved to be a cost-effective way to promote the efficient separation of charge carriers. For instance, our group has also successfully fabricated a series of composite photocatalysts by different physicochemical

hybridization approaches including $SiO_2/BiVO_4$ [30], TiO_2/PCN [31], WO_3/PCN [32] and $Bi_2O_2CO_3$/PCN [33] with enhanced photocatalytic activity for CH_3CHO photooxidation or CO_2 photoreduction, but it still remains a large gap for the practical application. Various Sillén-related $[Bi_2O_2]^{2+}$ layered materials can be obtained by interleaving with anion ions (such as Cl^-, Br^-, I^-, OH^-, NO_3^-, SO_4^{2-}, and CO_3^{2-}) [34]. Among these bismuth-based oxides, $Bi_2O_2(OH)(NO_3)$ (denoted as BION) is often used as nonlinear optical (NLO) material due to its non-centrosymmetric configuration [35]. Only just a few reports involved its photocatalytic applications so far [36, 37]. Thus we attempted to further enhance the photocatalytic activity of PCN by coupling it with the BION layered structure, because the spontaneous polarization in layered BION may greatly promote the separation of photogenerated charge carriers of PCN. Typically, pure-phase BION is difficult to prepare even if the reaction pH is rigorously regulated by basic solutions (such as KOH, NaOH and urea), attributing to its incomplete hydrolysis of bismuth nitrate [36,38]. Therefore, it is still huge challenging to design a facile route to synthesize BION with definite compositions.

Herein, we firstly fabricated rose-like BION with layer-assembled morphology by a solvothermal (ethanol/water) treatment. The structure of BION was further ascertained by XRD, TG and XPS. Then, in order to build a heterostructured photocatalyst, PCN carrier was introduced into the solvothermal reaction system. Surprisingly, the BION crystals were fully transformed to BIOC phase by ion exchange at relatively low concentration of bismuth salt precursor. With increasing the bismuth salt precursor to a high concentration, the BIOC and BION coexisted on PCN surface. PCN bulks play multi-roles in this ingenious one-pot method. It guarantees the negatively charged surface to anchor plentiful bismuth precursor salts. More importantly, solvothermal treatment affords a weak basic and sufficient CO_3^{2-} ions environment to promote the following ion exchange reaction between BION and BIOC. Gaseous acetaldehyde (CH_3CHO), as one of the representative indoor and environmental toxic volatile organic compounds (VOCs), was selected as model pollutant to evaluate the photocatalytic performance of BIOC@PCN. The 0.5BIOC@PCN sample presents optimal photocatalytic performance for CH_3CHO removal, which is 10, 6.5 and 2 times higher than that of the PCN-Bulk, BION and mechanical mixed BIOC/PCN counterparts, respectively. 67% gaseous 500 ppm CH_3CHO VOCs were converted

into CO_2 just within 24 hours under irradiation of energy saving LED lamp (central wavelength of 435 nm). Transient photocurrent response and EPR results further verified the validity of the established heterojunction of BIOC@PCN in facilitating the separation of charge carriers. Therefore, this study not only rendered a cost-effective route to fabricate BIOC@PCN nanohybrid photocatalysts with remarkable enhanced photooxidation capability, but also paves the way to develop other late-model and highly efficient bismuth-based and graphitic-based materials for photocatalysis.

2. Experimental Section

2.1. Materials

All of the reagents were of analytical grade and were used as received. Deionized water (18.4 MΩ, PURELAB flex3 water systems**)** was used in all of the experiments. Melamine (>99%) and Bismuth(Ⅲ) Nitrate pentahydrate $Bi(NO_3)_3•5H_2O$ (>98%) were purchased from Wako Pure Chemical Industries, Ltd. Acetaldehyde (ACS reagent Assay min 99.5%) was purchased from Sigma-Aldrich. It is extremely toxic and carcinogenic, and the use of personal protective equipment is required. Pure Air (CO_2<0.1ppm) was a product of Taiyo Nippon Sanso.

2.2. Preparation of samples

Polymeric carbon nitride was prepared according to the previously reported method with a slight modification [15]. Briefly, thirty grams of melamine were placed in an alumina crucible with a cover and then heated to 823 K with a ramping rate of 2.3 K min^{-1} in a temperature programming electric furnace (HPM-1G, AS ONE) and was kept at that temperature for 4 hours and then cooled to room temperature (RT). The obtained yellow bulk (ca.10 g) was ground into powder and is denoted as PCN-Bulk.

In a typical synthesis of BIOC@PCN, the above as-prepared PCN-Bulk (0.6g), specified molar ratio of $Bi(NO_3)_3•5H_2O$ (0mmol, 0.25mmol, 0.5mmol, 1.0mmol, 2.0mmol) were added to 100 ml Teflon reaction lined equipped with stainless steel autoclave. After dispersed in ethanol/water (1:1) mixed solvent for 2 h, the autoclave was transferred to an oven at 433 K for 18

h. After cooling, the residue was centrifuged, dried and ground. For simplification, the obtained products were denoted as PCN (m=0) and mBIOC@PCN (m=0.25, 0.5, 1.0, and 2.0). The controlled experiment was also carried out to prepare BION according with the same above procedure except addition of as-prepared PCN-Bulk powders.

In a typical synthesis of 0.5BIOC/PCN (mechanical force mixtures) photocatalyst, the above as-prepared PCN-Bulk (0.6 g) together with 0.15g BIOC was first mixed in 20 mL deionized water and then transferred to a 50 mL agate bowl containing 50 g yttrium-stabilized zirconia (YSZ) grinding beads (0.6 mm in diameter, Nikkato Co.,). The agate bowl was put on a planetary mill machine (Planetary Micro Mill pulverisette 7, Fritsch Japan Co.), operating at 750 rpm for 10 min with 3 repetitions. After cooling to RT, the YSZ beads could be moved by screening, and the sample was separated by filtration, washed with deionized water 3 times, and dried in a vacuum drying oven at 333 K overnight. These as-prepared samples were denoted as 0.5BIOC/PCN.

2.3. Characterization

X-ray diffraction (XRD) patterns of the as-prepared samples were recorded at room temperature by using a Rigaku diffactometer (MiniFlex-II, Japan) with Cu Kα irradiation (λ = 0.15418 nm), with an accelerating voltage of 30 kV and emission current of 15 mA. FTIR spectra were obtained on a JASCO FT/IR 4200 spectrometer with a DR-81 diffuse reflectance attachment. UV-vis diffuse reflectance spectra (DRS) of the samples were obtained by using a spectrometer (Shimadzu, UV-2600) with an integrating sphere accessory (Shimadzu, ISR-240A). $BaSO_4$ was used as a reference and adsorption spectra were calculated from reflectance data using the Kubelka-Munk function. Morphology information was obtained by using a scanning electron microscope (SEM, Jeol, JSM-6701F) and a high-resolution transmission electron microscope (HR-TEM, FEI, Tecnai G^2 F30 S-TWIN, 300 KV) equipped with EDX component. N_2 adsorption-desorption isotherms were recorded at 77 K on a surface area analyzer (Quantachrome, Nova 4200e). Specific surface area (S_{BET}) and pore size/volume were calculated from the Brunauer-Emmit-Teller (BET) theory and Barrett-Joyner-Halenda (BJH) theory, respectively.

Photoluminescence spectra (PL) of the samples were measured by a Jasco FP-8500 (Japan) spectrofluorometer at an excitation wavelength of 300 nm. Surface chemical states were investigated by X-ray photoelectron spectroscopy (XPS) measurement with a Shimadzu Kratos AXIS-NOVA system by Al Ka radiation and adventitious C1s peak (284.6 eV) as the reference. Electron paramagnetic resonance (EPR) radical signal was recorded by a Brucker EPR A200 spectrometer.

2.4. Photocatalytic evaluation experiments

2.4.1. Photooxidation of gaseous CH_3CHO

Before evaluation of the photocatalytic activity, all samples were irradiated with UV light using a black light lamp (UVP, XX-15BLB) overnight in order to remove organic contaminants on the surface. Then 0.1 g of a sample was tiled with good uniformity on the bottom of a watch-glass (φ=26.5 mm). The watch-glass was placed in a Tedlar bag (Polyvinyl fluoride, AS ONE Co., Ltd), then 125 mL of acetaldehyde/pure air mixture gas (500 ppm) were injected into the vacuumed bag. The bag was kept in a dark room for 2 h to establish the adsorption equilibrium between samples and acetaldehyde. Then the sample was irradiated by a light-emitting diode (LED, Epitex, and L435-30M32L) energy-saving lamp (central wavelength of 435 nm) with light intensity of 3 mW cm^{-2}. The variation in concentration of acetaldehyde and CO_2 evolution were monitored by on-line gas chromatography (Agilent Technologies, 3000A Micro-GC, TCD detector) with OV1 and PLOT-Q columns. The formate intermediates were detected by Ion Chromatography (DIONEX, ICS-900).

2.4.2. Photoelectrochemical measurements

The photoelectrodes were prepared by an electrophoretic deposition (EPD) method [5] on conducting FTO glass supports (Asahi Glass Co.). EPD was carried out in acetone (30 mL) containing photocatalysts powder (50 mg) and iodine (20 mg), which was dispersed by sonication for 15 min. Two FTO electrodes (1.5 X 4 cm^2) were immersed parallel in the solution with a distance of 10 mm, and 15 V of bias was then applied between the electrodes for 3 min using a

potentiostat (HAL-3001, Hokuto Denko Co.). The coated area was controlled to be ca. 1.5 X 2 cm^2. The electrode was dried in air on a digital hot plate (HP-1SA, As One Co.) at 473 K for 2 hours. Transient photocurrent response measurements of the as-prepared photoelectrodes were carried out by using an automatic polarization system (HSV-100, Hokuto Denko Co.) with a three-electrode system, in which the prepared electrode, a Pt electrode and a silver–silver chloride (Ag/AgCl) electrode were used as a working electrode, counter electrode and reference electrode, respectively. The electrolyte used was a 0.1 M Na_2SO_4 solution, which was bubbled with Ar gas for 30 min to remove dissolved air. The pH of the solution after bubbling was 6.8. The sample was irradiated by a 500 W Xe arc lamp (OPM2-502XQ, USHIO) with a heat-absorbing filter (Sigma Koki) and a 400 nm cutoff filter (Sigma Koki). The light intensity was measured to be 25 mW cm^{-2} (Orion-TH, Ophir Optronics).

3. Results and discussion

3.1 The morphology and structure of rose-like BION

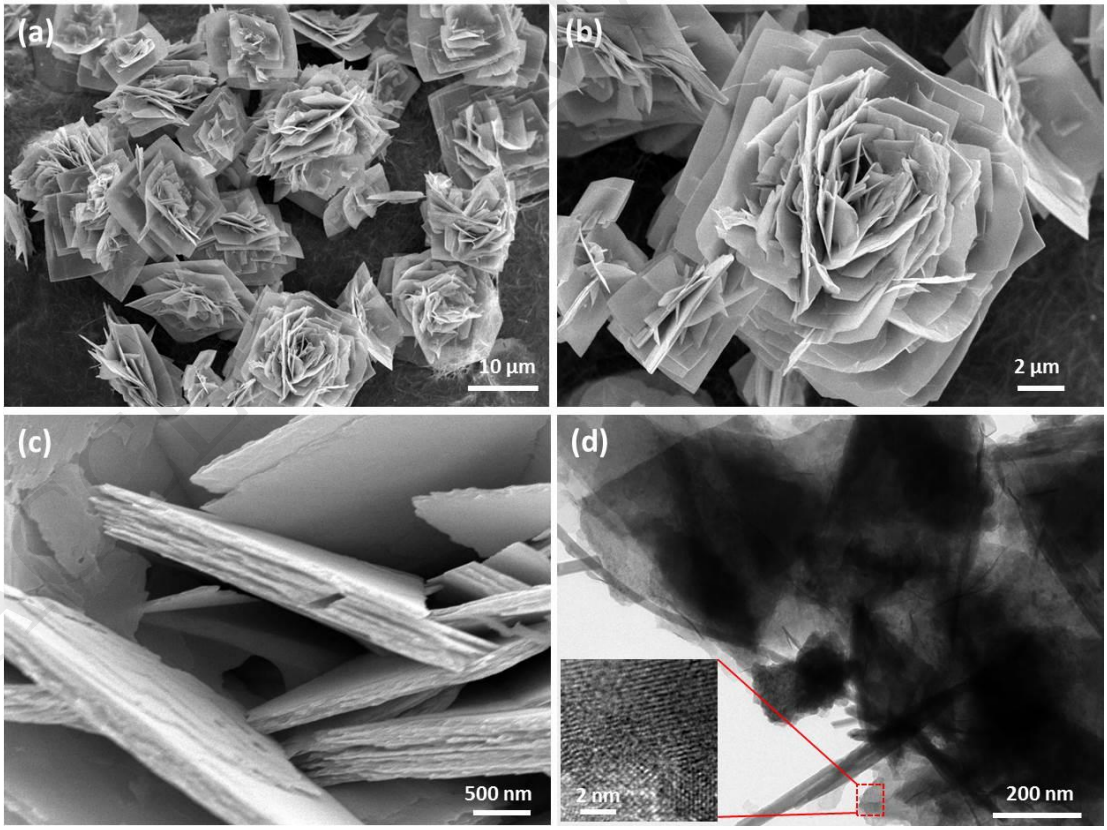

Figure 1. (a-c) SEM and (d) HR-TEM images of as-prepared rose-like BION.

The morphology and textural structure were observed by electron microscopy. FE-SEM images in Figure 1(a,b) indicate that uniform rose-like BION with base diameter of approximately 15 μm were obtained. The rose-like hierarchical microstructures are composed of numerous self-assembly nanosheets. The surface of the nanosheet is extremely smooth and flat. As given in Figure 1c, the nanosheet petals interleave with each other and individual nanosheets stack loosely with average thickness of 20 nm, illustrating the layered structure property of BION. HR-TEM image (Figure 1d and Figure S1) further reveals the lamination framework and single-crystal property of the as-prepared BION. The inset of Figure 1d shows clear lattice fringes with the interplanar spacings of 0.280 nm and 0.382 nm, ascribed to (114) and (110) planes of BION, respectively [37], implying the good crystalline of the as-prepared samples.

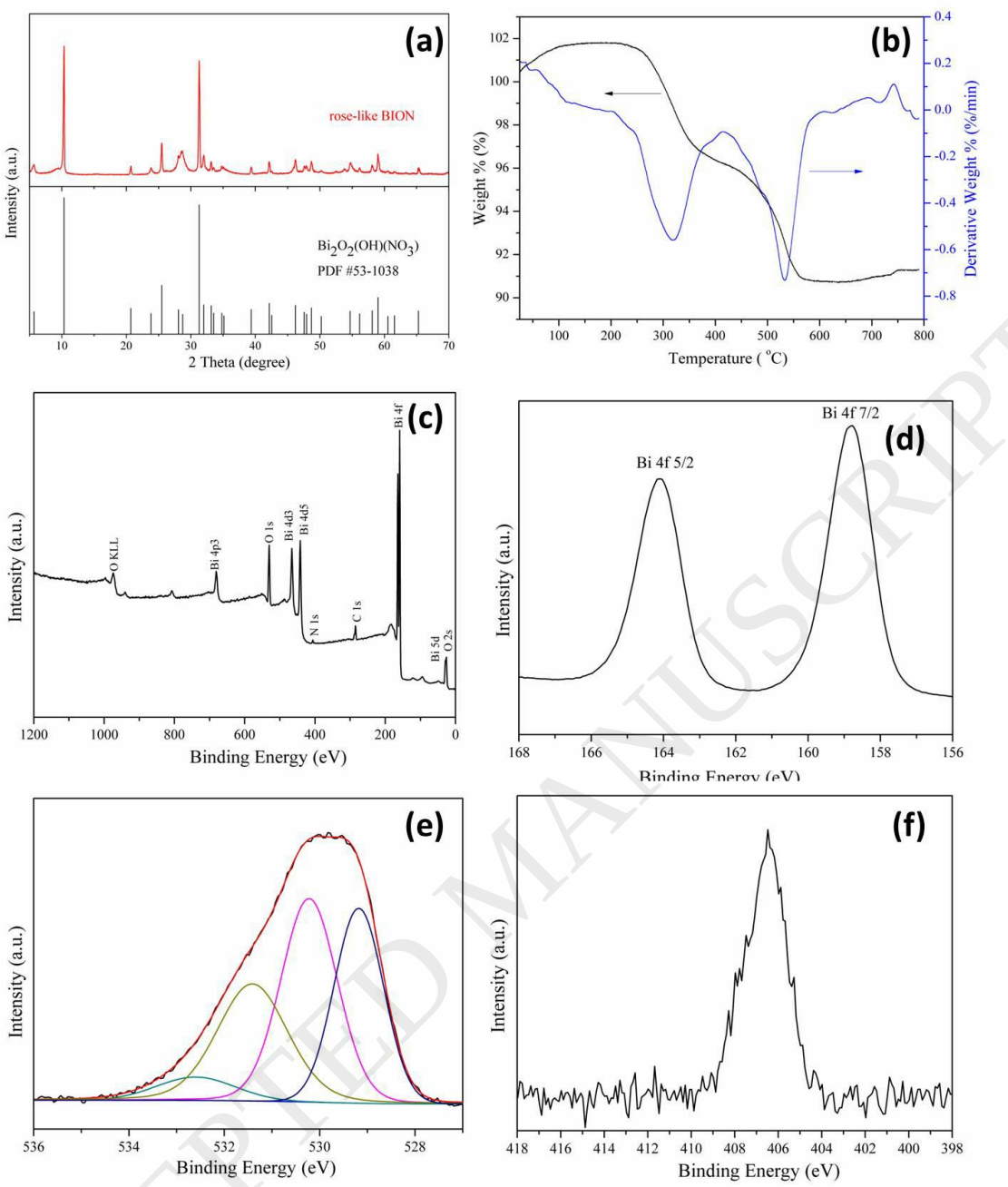

Figure 2. (a) XRD pattern; (b) TGA curve and (c-f) XPS spectra of the as-prepared rose-like BION: c) Survey, d) Bi 4f, e) O 1s and f) N1s.

Figure 2a shows the XRD pattern of the as-prepared rose-like BION. All the diffraction peaks can be well-indexed to orthorhombic $Bi_2O_2(OH)(NO_3)$ (PDF #53-1038 or ICSD #15-4359). The distinct peaks at 10.34°, 25.48°, 31.3° and 31.36° are assigned to (002), (112), (006) and (114) crystal planes of BION, respectively, matching well with the reported papers [36]. The diffraction peaks are sharp and strong, indicating its good crystallinity property, in accordance with HR-TEM

results. Besides, no impure peaks can be found, manifesting that the as-prepared rose-like BION is with high purity. Thermogravimetry analysis (TGA) has proved to be an effective technical means to acquire the molar mass and corresponding composition [38]. As displayed in Figure 2b, the mass of BION keeps constant value once heating temperature higher than 600 ºC, and the total weight loss rate of the as-prepared rose-like BION sample is 11.1%, approaching the theoretical weight loss rate 11.9%. It is worth noting that the weight loss rate (4.3%) between 530 ºC-630 ºC intervals meets perfectly with the following equation (1):

$$\mathbf{Bi_2O_2(OH)(NO_3)} \longrightarrow \mathbf{Bi_2O_3 + NO + 3/4\,O_2 + 1/2\,H_2O} \quad (\mathbf{1})$$

The surface chemical state of the as-prepared rose-like BION was investigated by XPS. Figure 2c shows the survey spectrum: the O, N and Bi come from BION and the additional carbon signal derives from amorphous carbon (284.6 eV). The high resolution XPS spectra of Bi 4f, O 1s and N 1s after deconvolution are given in Figure 2(d-f). The peaks at 164.08 eV and 158.78 eV are assigned to Bi $4f_{5/2}$ and Bi $4f_{7/2}$ of BIOC sample (Figure 2d). Meanwhile, these two symmetric peaks with well separated spin-orbit components (Δ=5.3 eV) further unfold the sample is a Bi^{3+} oxide. The O 1s core level of the sample could be fitted into four peaks (Figure 2e). Peaks located at 529.2 eV, 530.2 eV, 531.4 eV and 532.6 eV could be attributed to the Bi-O, NO_3^- , -OH and adsorbed O_2. The calculated peak area ratio of [Bi-O]:[OH+NO_3] is about 1:2, which fully confirms the chemical formula of the as-prepared material is $Bi_2O_2(OH)(NO_3)$. The N 1s peak located at 406.5 eV, belonging to NO_3^- anion (Figure 2f), which is in consistent with reported values [36,37].

3.2 The morphology and structure of BIOC@PCN

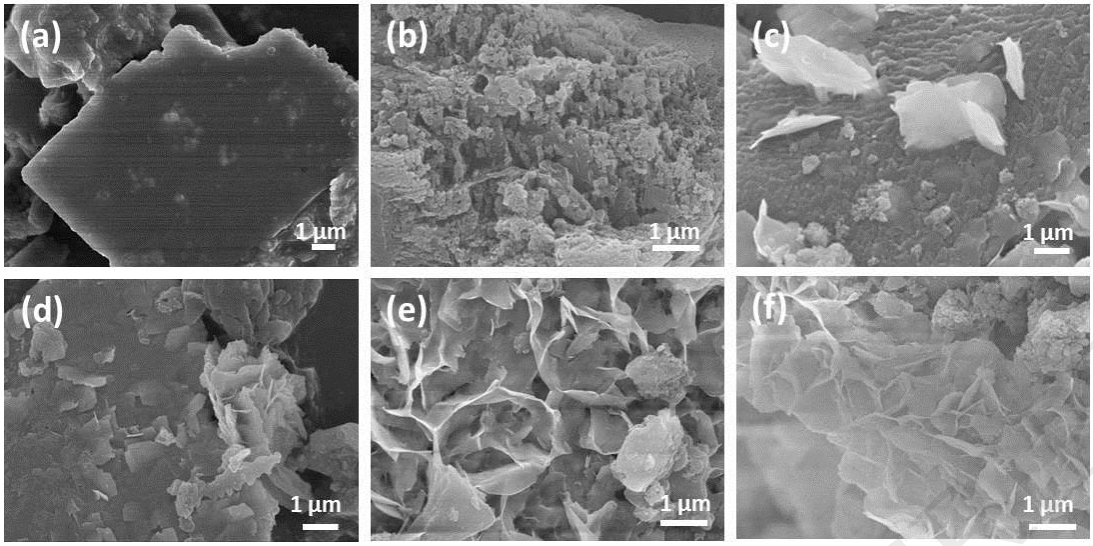

Figure 3. SEM images of as-prepared samples : (a) PCN-Bulk, (b) PCN, (c) 0.25BIOC@PCN, (d) 0.5BIOC@PCN, (e) 1.0BIOC@PCN and (f) 2.0BIOC@PCN.

The shape and size information of the as-prepared BIOC@PCN nanohybrid photocatalysts were obtained by scanning electron microscope, as shown in Figure 3. Figure 3a shows that PCN-Bulk synthesized from melamine has sheet-stacked structure and smooth surface with tens of microns. However, PCN bulks would be partially destroyed and peeled by ethanol/water mixed solvothermal treatment (as shown in Figure 3b). Simultaneously, the specific surface area of PCN is increased 3 times after solvothermal treatment (referred to Figure 5d and Figure S2), which is originated from breakdown of marginal $–NH_2$ and unstable zone from PCN matrix. The released NH_3 and CO_2 gases can introduce a great number of disordered micro/meso-pores, which is also well consistent with BET and BJH calculation results (Figure 5d and Figure S2). More importantly, we further verified the generation of NH_4^+ and CO_3^{2-} by addition of excessive $CaCl_2$ or NaOH solution into PCN supernatant solution after 18 h solvothermal treatment at 433K (as illustrated in Figure S3). By comparison with SEM images of Figure 3(c-f), we can draw the conclusion that with increasing the mole ratios of bismuth salts to the reaction system, the coverage fraction on PCN surface increased gradually by the in-situ-assembled nanosheets. In addition, the PCN substrate has a great influence on the final morphology of the as-prepared BIOC, changing from individual nanosheet to rose-like nanosheet assembles. The transformation from BION to BIOC is an ion exchange reaction, which is driven by the ions concentration difference

between CO_3^{2-} and NO_3^-. The number of CO_3^{2-} is with limited degree, because it is derived from hydrolyzation of unstable zone within PCN carrier [39]. Therefore, it is reasonable that BION can be fully converted into BIOC under low concentration of bismuth salts. Conversely, BION and BIOC would coexist on PCN surface with high concentration of bismuth salts. In detail, the negatively charged PCN sheets provide numerous "active-sites" for $[Bi_2O_2]^{2+}$ cations, so these metal ions can uniformly anchor on PCN surface, because isoelectric point (IEP) of PCN is 6.32 (measured by zeta potential, given in Figure S4). On the other hand, the slow-released CO_3^{2-} ions from the PCN combine with $[Bi_2O_2]^{2+}$ to form the BIOC deposition products. Moreover, the weak basic environment guarantees the growth and ripening of BIOC crystal grains to assemble as BIOC nanosheets on PCN surface. From SEM images in Figure 3, we can easily observe that the PCN nanosheets grow along the surface of PCN, because these zones are with high concentration CO_3^{2-} ions. Meanwhile, the in-situ formed nanosheets established an intimate contact with PCN substrate, which is beneficial to enhance the photogenerated charge carriers separation and transfer from PCN to BIOC. However, if the surface of PCN was fully covered by BIOC nanosheets or rose-like BION, it would greatly reduce the visible light absorption of PCN, thus there is an optimal deposition content (the bismuth salt addition in our system should be smaller than 1 mmol). The overall chemical reactions during the BIOC@PCN formation are listed in equation (2-7):

$$\mathbf{Bi(NO_3)_3 + H_2O \longrightarrow BiO(NO_3) + 2H^+ + 2NO_3^-} \quad (2)$$

$$\mathbf{2BiO(NO_3) + H_2O \longrightarrow Bi_2O_2(OH)(NO_3) + H^+ + NO_3^-} \quad (3)$$

$$\mathbf{PCN + H_2O \longrightarrow CO_2 + NH_3} \ \boldsymbol{(slow)} \quad (4)$$

$$\mathbf{NH_3 + H_2O \longrightarrow NH_4^+ + OH^-} \quad (5)$$

$$\mathbf{CO_2 + 2OH^- \longrightarrow CO_3^{2-} + H_2O} \quad (6)$$

$$\mathbf{Bi_2O_2(OH)(NO_3) + CO_3^{2-} \longrightarrow Bi_2O_2CO_3\downarrow + OH^- + NO_3^-} \quad (7)$$

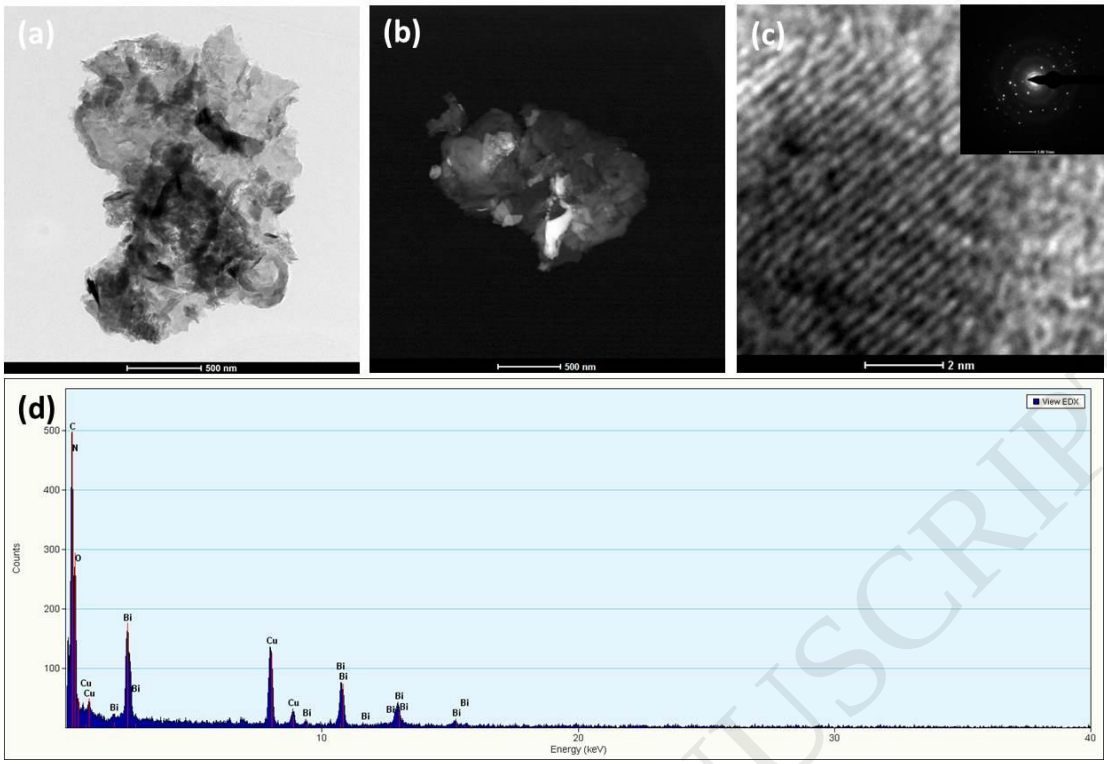

Figure 4. Morphology characterization of 0.5BIOC@PCN sample: (a) TEM, (b) HAADF, (c) HR-TEM with SAED inset and (d) EDX.

Only by SEM images, it is really difficult to distinguish fair or foul of the asserted BIOC@PCN heterojunction structure. Thus, a much more powerful instrument, HR-TEM, was selected to work out this keypoint. Four modes of HR-TEM, HAADF, SAED and EDX characterization results for 0.5BIOC@PCN are shown in Figure 4. TEM images and high angle annular dark filed (HAADF) image in Figure 4(a,b) obviously illustrated BIOC nanosheets are with good distribution on PCN. Namely, the dark part in Figure 4a and the bright one in Figure 4b present only the BIOC component, because the contrast intensity of HAADF is in direct proportion to the square value of atomic number. As given in Figure 4c, BIOC nanosheets were indeed embedded into the flexible and multiporous PCN matrix to establish an intimated and well-defined heterojunction interfacial structure, endowing lattice deformation between BIOC and PCN crystal boundary. Besides, the in-situ formed BIOC nanosheets show a single-crystal phase with exposed (013) facets (d_{space}=0.296 nm). EDX measurement (Figure.4d) further revealed the BIOC@PCN nanohybrids were exactly composed of C, N, O and Bi elements, while the Cu signal

derived from the Cu grids. Therefore, this one-pot solvothermal treatment has turned out to be a feasible approach to fabricate BIOC@PCN heterojunction photocatalysts.

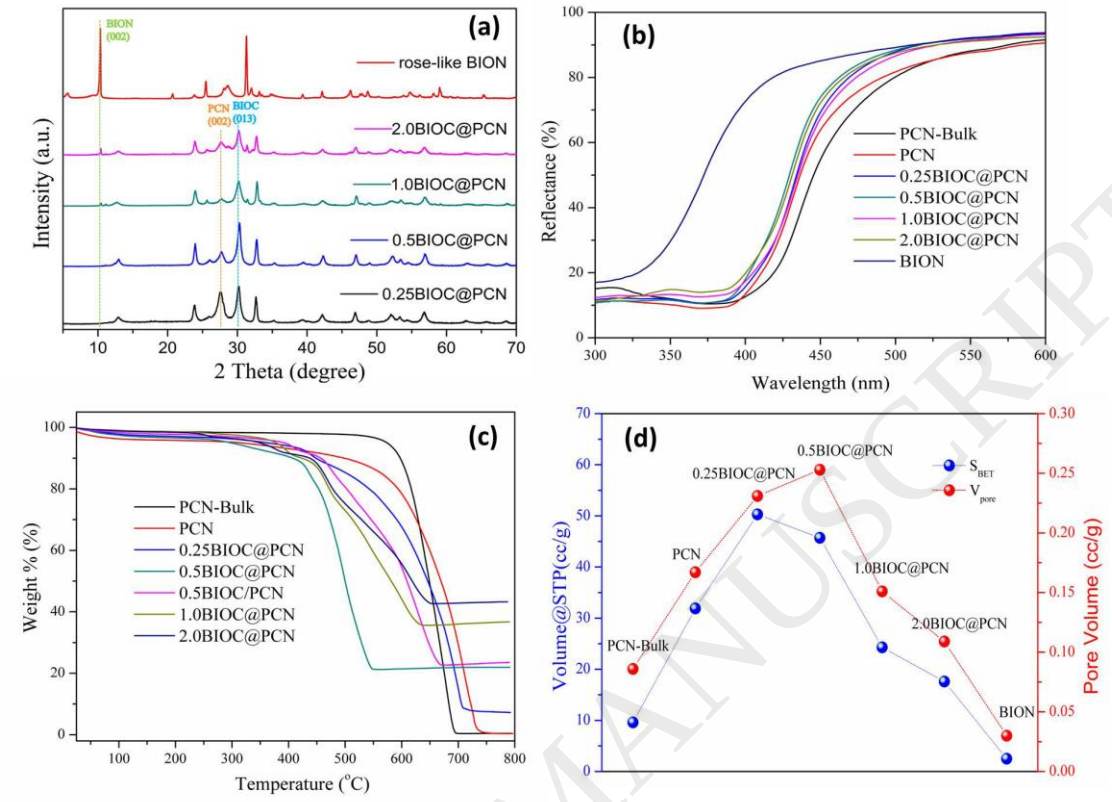

Figure 5. Structure characterization of BIOC@PCN samples: (a) XRD, (b) UV-vis, (c) TGA and (d) BET&BJH.

Figure 5a and Figure S5 show the XRD patterns of a series of as-prepared BIOC@PCN samples. The diffraction peaks of PCN-Bulk and PCN (Figure S6) at 27.4° can be indexed as (002) facets, which corresponds to distance of aromatic segments interlayer stacking (d=0.326 nm), which also matches well with literature reported values (JCPDS 87-1526) [10]. The peaks of $Bi_2O_2CO_3$ (BIOC) are well assigned to tetragonal crystal phase (JCPDS 41-1488). As the addition of bismuth salts exceeds 1mmol, the characteristic peaks at 10.33°, 25.47°, 31.29° of $Bi_2O_2(OH)(NO_3)$ (BION) crystal phase (PDF #53-1038 or ICSD #15-4359) appear, coexisting with BIOC on PCN. By analysis of the XRD patterns, we can also conclude that with increasing of bismuth salts amount, the PCN surface was gradually covered by generated BIOC (or BION), because the peak intensity of PCN at (002) became weaken in BIOC@PCN. The XRD results are

also well in accordance with SEM images shown in Figure 3. Figure 5b exhibits the diffuse reflectance spectra of BIOC@PCN. It indicates that the pure BION shows relatively weak visible response, while hybridized with PCN, BIOC@PCN heterojunction photocatalysts display obvious red-shift to visible light region compared with pure BION ones. In order to make clear the exact content of BIOC (or BION) in composite photocatalysts, TGA measurements were conducted (Figure 5c). The results show that the content of BIOC wt% in BIOC@PCN alters from 7%, 24%, 25%, 37% and 43% in the hybrid of 0.25BIOC@PCN, 0.5BIOC@PCN, 0.5BIOC/PCN, 1.0BIOC@PCN and 2.0BIOC@PCN, respectively. Moreover, the specific surface area and total pore volume are also depicted in Figure 5d, indicating that the S_{BET} and V_{pore} of BIOC@PCN were greatly enlarged by this one-pot solvothermal treatment, especially for 0.25BIOC@PCN and 0.5BIOC@PCN samples. Because at the low bismuth salts amount, the as-formed BION hierarchical microstructures were fully converted into dispersed BIOC nanosheets anchored on PCN with higher SBET, achieved by ion exchange reaction. As it has discussed earlier, the number of CO_3^{2-} is with limited degree, because it is derived from hydrolyzation of unstable zone from PCN carrier. But at the high concentrations of bismuth salts, only part of BION could be converted into BIOC, meaning BION and BIOC coexisted on PCN surface with lower S_{BET}. Besides, morphology and structure characterizations (given in Figures 1-5) adequately illustrated above-mentioned evolution process. Therefore, 0.25BIOC@PCN and 0.5BIOC@PCN samples presented higher specific surface area and pore volume values than other samples.

3.3 Evaluation of photocatalytic activity and proposed mechanism

Figure 6a presents the time courses of CO_2 evolution during the CH_3CHO degradation under visible light irradiation (LED 435 nm). Because the initial CH_3CHO concentration was 500 ppm (volume of 125 mL), 1000 ppm CO_2 would be generated once it was fully oxidized. Due to the small specific surface area and weak visible absorption ability, BION shows extremely weak photooxidation ability for conversion CH_3CHO to CO_2, and only 105 ppm of CO_2 were generated after 24 hours of visible light irradiation, PCN-Bulk also presents weak CH_3CHO abatement capability (66 ppm of CO_2 generated after 24h) because the strong recombination rate of photogenerated charge carriers in the bulk and the relatively slow adsorption on reaction active sites greatly impeded the enhancement of photocatalytic performance. The slow descending

tendencies of CH_3CHO variation curves for BION and PCN-Bulk shown in Figure S7 are the best circumstantial evidence of the above-mentioned inference. Results of blank experiments confirmed that the self-photolysis of CH_3CHO and self-photodecomposition of photocatalysts were both negligible. Once coupling PCN with BIOC nanosheets, the photooxidation abilities are boosted greatly. From Figure 6a, we can conclude that the 0.5BIOC@PCN nanohybrid photocatalyst displays the highest CO_2 generation concentration (670 ppm), which is 10, 6.5 and 2 times higher than that of PCN-Bulk, BION and mechanical mixed BIOC/PCN counterparts, respectively. $Bi_2O_2CO_3$@PCN fabricated by ion exchange in this study presented conspicuously superior activity for acetaldehyde oxidation than that of commercial metal oxide photocatalysts (such as P25, S-doped TiO_2, WO_3 and $Bi_2O_2CO_3$) and corresponding elaborate PCN-based nanocomposites, as compared in Table S1.

Table 1 Rate constants, initial degradation rates, C balances and percentages of mineralization for the CH_3CHO photooxidation to CO_2

Sample	Rate constant for CO_2 κ (h^{-1})	Initial degradation rate $-r_0\times10^6$ (mM m h^{-1})	C balance (%) at t =24 h	Mineralization (%) at t =24 h
PCN-Bulk	0.00148	0.01927	50	7
PCN	0.01234	0.04835	55	31
0.25BIOC@PCN	0.05410	0.13444	66	66
0.5BIOC@PCN	0.05777	0.15801	67	67
0.5BIOC/PCN	0.01456	0.08426	42	33
1.0BIOC@PCN	0.02422	0.12459	51	51
2.0BIOC@PCN	0.01572	0.11165	37	37
BION	0.00178	0.08900	42	11

Besides, according to the Langmuir-Hinshelwood rate law, the good linearity of the slopes of the CO_2 rate constants (Figure S8) indicates that the CH_3CHO degradation in this system followed a pseudo-first-order kinetics. Thus the reaction rate constants (κ) and the initial reaction rates ($-r_0$) for CO_2 derived from the CH_3CHO photooxidation were also calculated. The results were

summarized in Table 1. The initial degradation rate, $-r_0$, has been determined by the following equation (1):

$$(-r_0) = \left(-\frac{1}{S}\frac{dN}{dt}\right) = \left(-\frac{V}{S}\frac{dC}{dt}\right) \quad (1)$$

in which N represents the substrate moles, t is the irradiation time, S is the specific surface area, V is the suspension volume and C is the substrate concentration. It must be noted that the value of ($-r_0$) is independent of the surface area of catalyst and therefore it is a reliable parameter for evaluating the intrinsic catalyst activity [40]. The as-prepared $Bi_2O_2CO_3$@PCN presented much higher $-r_0$ and κ values than that of $Bi_2O_2CO_3$/PCN and individual counterparts, further indicating the intrinsic activity of the $Bi_2O_2CO_3$@PCN nanohybrid photocatalyst. The photocatalytic performance improvement of BIOC@PCN is mainly attributed to two reasons. On the one hand, the greatly enlarged S_{BET} (increased at least 3 times) as well as the formed numerous mesopores (pore volume changed from PCN-Bulk 0.086 cc/g to PCN 0.167cc/g) in PCN contributed better CH_3CHO adsorption ability. The in-situ assembled BIOC nanosheets further enlarged the S_{BET} and V_{Pore} of 0.5BIOC@PCN to 50.3 m^2/g and 0.231 cc/g with numerous mesopores (given in Figure 5d, Figure S9). On the other hand, the BIOC nanosheets show intimate contact with the PCN substrate, which is beneficial to separate photogenerated electrons from PCN to BIOC. Therefore, much more photogenerated holes and electrons prefer to be involved in the photooxidation reaction rather than annihilate by the form of radiation, which was further proved by PL spectra (Figure 6b) and photoelectrochemical measurement (Figure 6c). PL has turned out to be a powerful tool to probe the transfer, separation and recombination processes of photogenerated charge carriers. As given in Fig.6 (b), the PL intensity of PCN was much weaker than that of PCN-Bulk, indicating that hydrothermal treatment is an efficient way to remove the unstable zones and defects from PCN matrix, which may be the recombination center for charge carriers. After further hybridization with BIOC (referred to BIOC/PCN and BIOC@PCN), the photoinduced electrons can transfer smoothly from CB of PCN to CB of BIOC, indicating much more efficient separation routes of photoinduced electron-hole pairs were established. Moreover, BIOC@PCN sample presented superior promotion effect for the charge carriers than that of BIOC/PCN and PCN counterparts, attributing to the well-established heterojunction. The transient

photocurrent response curves (Figure 6c) show that the 0.5BIOC@PCN heterojunction photocatalyst have the highest photocurrent response under visible light irradiation (400 nm cutoff), which is about 3 and 8 times larger than that of the PCN and PCN-Bulk counterparts. However, as the addition content of bismuth salts exceeded the optimal value, the photocatalytic performance of the as-obtained BIOC@PCN hybridized photocatalysts was gradually reduced, ascribed to the weakened visible light adsorption and diminished total pore volume.

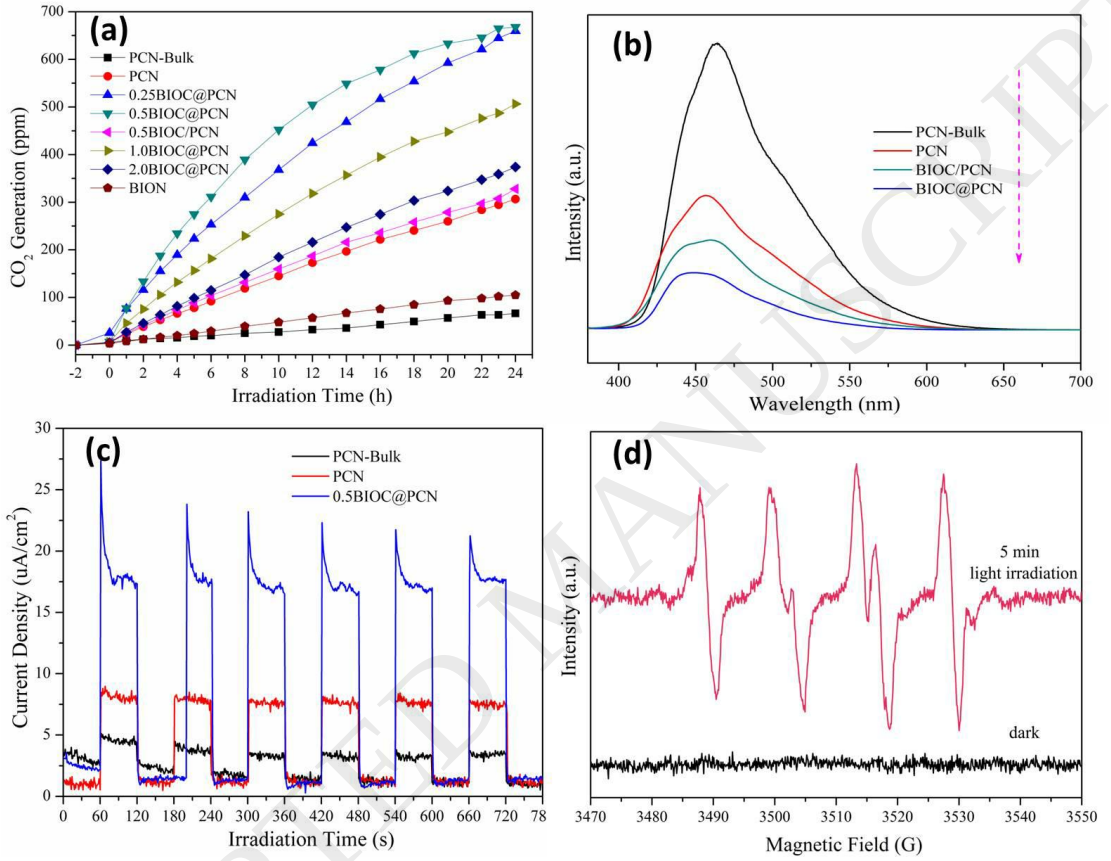

Figure 6. (a) Photocatalytic activity for CH_3CHO to CO_2, (b) PL spectra, (c) Transient photocurrent response curves and (d) EPR spectra.

The C balance and mineralization from CH_3CHO to CO_2 results of as-prepared photocatalysts were also given in Table 1. Taking into account only the unreacted CH_3CHO and the produced CO_2, the C balance and mineralization of 0.5BIOC@PCN demonstrated the optimal value among all the samples, reached to 70%. However, it is still below 100%, attributing to the adsorbed CH_3CHO and generated C-containing intermediates (such as HCOOH, CH_3COOH and

HCHO). By Ion Chromatography, formate intermediates were successfully detected on 0.5BIOC@PCN sample, as given in Figure S10a. Moreover, proposed conversion pathways for CH_3CHO photooxidation to CO_2 were also illustrated in Figure S10b.

Typically, a potential practical photocatalyst should possess good stability and renewable ability. Under the same conditions as those for the above activity evaluation, five cyclic experiments using the 0.5BIOC@PCN photocatalyst were also conducted (Figure S11), displaying a negligible activity loss. The 0.5BIOC@PCN sample after 120 hours of photocatalytic tests were also evaluated by FTIR and XRD, (shown in Figure S12 and Figure S13). Apart from anchoring of minor generated CO_2 and removal of trace adsorbed H_2O, there was no obvious changes in crystal structure and functional groups after visible light irradiation for such long time, providing convincing evidence of the outstanding stability of this heterojunction photocatalyst.

Although BIOC has negligible visible light-driven ability, the photogenerated electrons excited by PCN could be injected into the conduction band (CB) of BIOC to promote the separation of charge carries. The separation efficiency depended greatly on the quality/quantity of the heterojunction and the CB offset value. BIOC is a direct bandgap semiconductor with the CB position at 0.2 eV (vs. NHE), while the VB and CB of PCN are located at 1.5 and −1.2 eV (vs.NHE), respectively [41, 42]. The CB of BIOC is much more positive than that of PCN, accounting for the thermodynamically favorable process of the injection of such photogenerated electrons. On the other hand, a good nanosheets heterojunction between PCN and BIOC was established by one-pot solvothermal treatment and can further accelerate the transfer and separation of photoinduced charge carries in PCN. Based on the above-described structure characterization and results of evaluation of photocatalytic performance, an illustration scheme of the formation process and photocatalytic mechanism for the BIOC@PCN heterojunction photocatalyst is depicted in Figure 7. In such a hybridized system, only the PCN polymeric semiconductor can be excited under visible light irradiation. Then photogenerated electrons in the CB of PCN are continuously injected to the CB of BIOC. The established BIOC@PCN heterojunction structure can greatly promote the separation efficiency of charge carriers, as proved

by PL and transient photocurrent response. Specifically, in order to further make clear of the photocatalytic mechanism, the reactive oxygen species (ROS) H_2O_2 was successfully detected by EPR. As shown in Figure 6d, after 5 min light irradiation, strong H_2O_2 signal peaks were captured. Since the redox potential of $H_2O/\cdot OH$ (E=2.4 eV vs NHE) is much higher than the VB of PCN, it is very difficult to generate ·OH in the BIOC@PCN system, while $O_2/\cdot O_2^-$ (E=-0.16 eV vs NHE) is prone to proceed. Actually, the generated H_2O_2 is a highly efficient intermediate with redox ability to further promote the improvement of photocatalytic activity, as proposed in the schematic illustration of Figure 7. Therefore, the dramatically enhanced photocatalytic performance of the BIOC@PCN nanohybrid is finally attributed to the synergistic effect of established heterojunction, enlarged surface area/mesopores and the generated H_2O_2.

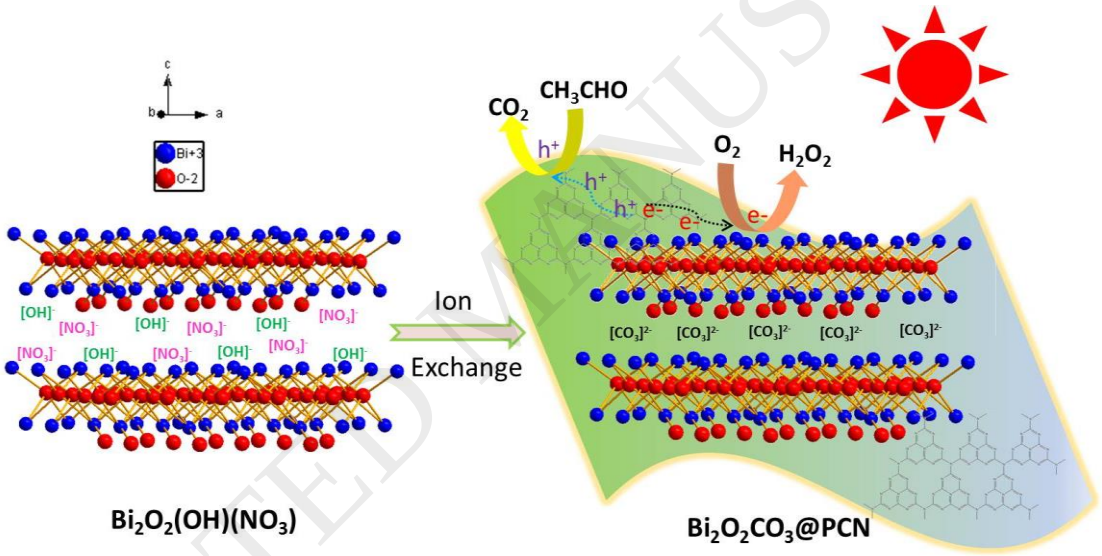

Figure 7. Illustration scheme of BIOC@PCN formation and its photocatalytic mechanism.

4. Conclusions

In summary, we developed a facile and cost-effective in-situ method to fabricate BIOC@PCN heterojunction photocatalysts by ion exchange between rose-like BION and PCN bulks at 433 K solvothermal condition. The photocatalytic performance of the as-prepared samples for degrading gaseous CH_3CHO under visible light irradiation was systemically evaluated. Various characterizations were adopted to disclose the structure-function relationship. The as-prepared

nanohybrid photocatalyst (0.5BIOC@PCN) presents outstanding photocatalytic performance for gaseous acetaldehyde removal, showing 10, 6.5 and 2 times higher than that of PCN-Bulk, BION and mechanical force mixtures BIOC/PCN counterparts, respectively. Transient photocurrent response and EPR results further verify the validity of the established heterojunction of BIOC@PCN in facilitating the separation of charge carriers. Therefore, this study not only rendered a cost-effective route to fabricate BIOC@PCN nanohybrid photocatalysts with remarkable enhanced photooxidation capability, but also paves the way to develop other late-model and highly efficient bismuth-based and graphitic-based materials for photoelectrocatalysis.

Acknowledgements

This work was financially supported by JST ACT-C program of Japan and National Natural Science Foundation of China (Grant No. 21506126 and 51502174). The authors also express their sincere thanks for the grant provided by the Science and Technology Project of Shenzhen (Grant Nos.JCYJ20150324141711616, JCYJ20150324141711645), and the Natural Science Foundation of Shenzhen University (Grant No. 827-000059), the Major Projects of Nature Science Research in Universities and Colleges in Jiangsu Province, China (No. 16KJA150008)

Appendix A. Supplementary data

Supplementary data associated with this article can be found, in the online version.

References

[1] A. Fujishima, K. Honda, Electrochemical Photolysis of Water at a Semiconductor Electrode. Nature 238 (1972) 37-38.
[2] R.W. Matthews, Kinetics of photocatalytic oxidation of organic solutes over titanium dioxide. Journal of Catalysis 111 (1988) 264-272.
[3] V.M. Menéndez-Flores, T. Ohno, High visible-light active Ir-doped-TiO_2 brookite photocatalyst synthesized by hydrothermal microwave-assisted process. Catalysis Today 230 (2014) 214-220.
[4] O. Carp, C.L. Huisman, A. Reller, Photoinduced reactivity of titanium dioxide. Progress in Solid State Chemistry 32 (2004) 33-177.
[5] S.N. Habisreutinger, L. Schmidt-Mende, J.K. Stolarczyk, Photocatalytic reduction of CO_2 on TiO2 and other semiconductors. Angewandte Chemie International Edition 52 (2013) 7372-7408.
[6] G. Liu, L.-C. Yin, J. Wang, P. Niu, C. Zhen, Y. Xie, H.-M. Cheng, A red anatase TiO_2 photocatalyst for solar energy conversion. Energy & Environmental Science 5 (2012) 9603-9610.

[7] X. Xin, T. Xu, L. Wang, C. Wang, Ti^{3+}-self doped brookite TiO_2 single-crystalline nanosheets with high solar absorption and excellent photocatalytic CO_2 reduction. Scientific reports 6 (2016) 23684.
[8] A. Naldoni, M. Allieta, S. Santangelo, M. Marelli, F. Fabbri, S. Cappelli, C.L. Bianchi, R. Psaro, V. Dal Santo, Effect of Nature and Location of Defects on Bandgap Narrowing in Black TiO_2 Nanoparticles. Journal of the American Chemical Society 134 (2012) 7600-7603.
[9] C. Su, R. Tandiana, B. Tian, A. Sengupta, W. Tang, J. Su, K.P. Loh, Visible-Light Photocatalysis of Aerobic Oxidation Reactions Using Carbazolic Conjugated Microporous Polymers, ACS Catalysis 6 (2016) 3594-3599.
[10] X. Wang, K. Maeda, A. Thomas, K. Takanabe, G. Xin, J.M. Carlsson, K. Domen, M. Antonietti, A metal-free polymeric photocatalyst for hydrogen production from water under visible light. Nature Materials 8 (2009) 76-80.
[11] J. Liu, Y. Liu, N. Liu, Y. Han, X. Zhang, H. Huang, Y. Lifshitz, S.-T. Lee, J. Zhong, Z. Kang, Metal-free efficient photocatalyst for stable visible water splitting via a two-electron pathway. Science 347 (2015) 970-974.
[12] X.-H. Li, X. Wang, M. Antonietti, Solvent-Free and Metal-Free Oxidation of Toluene Using O_2 and g-C_3N_4 with Nanopores: Nanostructure Boosts the Catalytic Selectivity. ACS Catalysis 2 (2012) 2082-2086.
[13] G. Gao, Y. Jiao, E.R. Waclawik, A. Du, Single Atom (Pd/Pt) Supported on Graphitic Carbon Nitride as an Efficient Photocatalyst for Visible-Light Reduction of Carbon Dioxide. Journal of the American Chemical Society 138 (2016) 6292-6297.
[14] F.K. Kessler, Y. Zheng, D. Schwarz, C. Merschjann, W. Schnick, X. Wang, M.J. Bojdys, Functional carbon nitride materials-design strategies for electrochemical devices. Nature Review Materials 2 (2017) 17030.
[15] G. Gunniya Hariyanandam, D. Hyun, P. Natarajan, K.-D. Jung, S. Yoon, An effective heterogeneous Ir(III) catalyst, immobilized on a heptazine-based organic framework, for the hydrogenation of CO_2 to formate. Catalysis Today 265 (2016) 52-55.
[16] S. Hu, R. Jin, G. Lu, D. Liu, J. Gui, The properties and photocatalytic performance comparison of Fe^{3+}-doped g-C_3N_4 and Fe_2O_3/g-C_3N_4 composite catalysts. RSC Advances 4 (2014) 24863-24869.
[17] S. Hu, F. Li, Z. Fan, F. Wang, Y. Zhao, Z. Lv, Band gap-tunable potassium doped graphitic carbon nitride with enhanced mineralization ability. Dalton Transactions 44 (2015) 1084-1092.
[18] S. Hu, L. Ma, J. You, F. Li, Z. Fan, G. Lu, D. Liu, J. Gui, Enhanced visible light photocatalytic performance of g-C_3N_4 photocatalysts co-doped with iron and phosphorus. Applied Surface Science 311 (2014) 164-171.
[19] G. Zhang, M. Zhang, X. Ye, X. Qiu, S. Lin, X. Wang, Iodine Modified Carbon Nitride Semiconductors as Visible Light Photocatalysts for Hydrogen Evolution. Advanced Materials 26 (2014) 805-809.
[20] K. Li, S. Gao, Q. Wang, H. Xu, Z. Wang, B. Huang, Y. Dai, J. Lu, In-Situ-Reduced Synthesis of Ti^{3+} Self-Doped TiO_2/g-C_3N_4 Heterojunctions with High Photocatalytic Performance under LED Light Irradiation. ACS Applied Materials & Interfaces 7 (2015) 9023-9030.
[21] A. Akhundi, A. Habibi-Yangjeh, Ternary g-C_3N_4/ZnO/AgCl nanocomposites: Synergistic collaboration on visible-light-driven activity in photodegradation of an organic pollutant. Applied Surface Science 358, Part A (2015) 261-269.
[22] A. Akhundi, A. Habibi-Yangjeh, Ternary magnetic g-C_3N_4/Fe_3O_4/AgI nanocomposites: Novel recyclable photocatalysts with enhanced activity in degradation of different pollutants under visible light. Materials Chemistry and Physics 174 (2016) 59-69.
[23] A. Habibi-Yangjeh, A. Akhundi, Novel ternary g-C_3N_4/Fe_3O_4/Ag_2CrO_4 nanocomposites: magnetically separable and visible-light-driven photocatalysts for degradation of water pollutants. Journal of Molecular Catalysis A: Chemical 415 (2016) 122-130.
[24] M. Mousavi, A. Habibi-Yangjeh, Magnetically separable ternary g-C_3N_4/Fe_3O_4/BiOI nanocomposites: Novel visible-light-driven photocatalysts based on graphitic carbon nitride. Journal of Colloid and Interface Science 465 (2016) 83-92.
[25] L. Shi, L. Liang, J. Ma, F. Wang, J. Sun, Enhanced photocatalytic activity over the Ag_2O-g-C_3N_4 composite under visible light. Catalysis Science & Technology 4 (2014) 758-765.

[26] L. Shi, L. Liang, J. Ma, F. Wang, J. Sun, Remarkably enhanced photocatalytic activity of ordered mesoporous carbon/g-C_3N_4 composite photocatalysts under visible light. Dalton Transactions 43 (2014) 7236-7244.
[27] L. Shi, L. Liang, F. Wang, M. Liu, S. Zhong, J. Sun, Tetraethylorthosilicate induced preparation of mesoporous graphitic carbon nitride with improved visible light photocatalytic activity. Catalysis Communications 59 (2015) 131-135.
[28] Q. Han, B. Wang, J. Gao, Z. Cheng, Y. Zhao, Z. Zhang, L. Qu, Crystalline Carbon Nitride Nanosheets for Improved Visible-Light Hydrogen Evolution. ACS Nano 10 (2016) 2745-2751.
[29] X. Zhang, X. Xie, H. Wang, J. Zhang, B. Pan, Y. Xie, Enhanced Photoresponsive Ultrathin Graphitic-Phase C_3N_4 Nanosheets for Bioimaging. Journal of the American Chemical Society 135 (2013) 18-21.
[30] N. Murakami, N. Takebe, T. Tsubota, T. Ohno, Improvement of visible light photocatalytic acetaldehyde decomposition of bismuth vanadate/silica nanocomposites by cocatalyst loading. Journal of Hazardous Materials 211-212 (2012) 83-87.
[31] K. Kondo, N. Murakami, C. Ye, T. Tsubota, T. Ohno, Development of highly efficient sulfur-doped TiO_2 photocatalysts hybridized with graphitic carbon nitride. Applied Catalysis B: Environmental 142-143 (2013) 362-367.
[32] Z. Jin, N. Murakami, T. Tsubota, T. Ohno, Complete oxidation of acetaldehyde over a composite photocatalyst of graphitic carbon nitride and tungsten(VI) oxide under visible-light irradiation. Applied Catalysis B: Environmental 150-151 (2014) 479-485.
[33] Q. Zhang, B. Xu, S. Yuan, M. Zhang, T. Ohno, Improving g-C_3N_4 photocatalytic performance by hybridizing with $Bi_2O_2CO_3$ nanosheets, Catalysis Today 284 (2017) 27-36.
[34] H. Tian, F. Teng, J. Xu, S. Lou, N. Li, Y. Zhao, M. Chen, An Innovative Anion Regulation Strategy for Energy Bands of Semiconductors: A Case from Bi_2O_3 to $Bi_2O(OH)_2SO_4$. Scientific Reports 5:7770 (2015) 1-9.
[35] C. Wang, Q. Liu, Z. Li, A new nonlinear optical crystal: $Bi_2O_2(OH)(NO_3)$, Crystal Research and Technology 46 (2011) 655-658.
[36] H. Huang, Y. He, X. Li, M. Li, C. Zeng, F. Dong, X. Du, T. Zhang, Y. Zhang, $Bi_2O_2(OH)(NO_3)$ as a desirable $[Bi_2O_2]^{2+}$ layered photocatalyst: strong intrinsic polarity, rational band structure and {001} active facets co-beneficial for robust photooxidation capability. Journal of Materials Chemistry A 3 (2015) 24547-24556.
[37] Q. Han, J. Pang, X. Wang, X. Wu, J. Zhu, Synthesis of Unique Flowerlike $Bi_2O_2(OH)(NO_3)$ Hierarchical Microstructures with High Surface Area and Superior Photocatalytic Performance. Chemistry-A European Journal 23 (2017) 3891-3897.
[38] N. Henry, M. Evain, P. Deniard, S. Jobic, F. Abraham, O. Mentré, $[Bi_2O_2]^{2+}$ Layers in $Bi_2O_2(OH)(NO_3)$: Synthesis and Structure Determination. Zeitschrift für Naturforschung B, 2005, 322-327.
[39] Sano, T., Tsutsui, S., Koike, K., Hirakawa, T., Teramoto, Y., Negishi, N., Takeuchi, K., Activation of graphitic carbon nitride (g-C_3N_4) by alkaline hydrothermal treatment for photocatalytic NO oxidation in gas phase. Journal of Materials Chemistry A 1 (2013) 6489-6496.
[40] S. Yurdakal, V. Augugliaro, Partial oxidation of aromatic alcohols via TiO_2 photocatalysis: the influence of substituent groups on the activity and selectivity, RSC Advances 2 (2012) 8375-8380.
[41] N. Tian, H. Huang, Y. Guo, Y. He, Y. Zhang, A g-C_3N_4/$Bi_2O_2CO_3$ composite with high visible-light-driven photocatalytic activity for rhodamine B degradation. Applied Surface Science 322 (2014) 249-254.
[42] S.C. Yan, Z.S. Li, Z.G. Zou, Photodegradation Performance of g-C_3N_4 Fabricated by Directly Heating Melamine. Langmuir 25 (2009) 10397-10401.